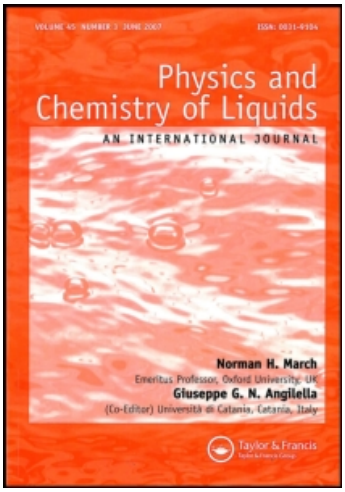


**Physics and Chemistry of Liquids**
Publication details, including instructions for authors and subscription information:
http://www.informaworld.com/smpp/title~content=t713646857

# Association and molecular chain length effects on interfacial behavior

A. Mejía[a]; H. Segura[a]; J. Wisniak[b]; I. Polishuk[b]
[a] Departamento de Ingeniería Química, Universidad de Concepción, Concepción, Chile [b] Department of Chemical Engineering, Ben-Gurion University of the Negev, Beer-Sheva 84105, Israel

**To cite this Article** Mejía, A. , Segura, H. , Wisniak, J. and Polishuk, I.(2006) 'Association and molecular chain length effects on interfacial behavior', Physics and Chemistry of Liquids, 44: 1, 45 — 59
**To link to this Article: DOI:** 10.1080/00319100500303304
**URL:** http://dx.doi.org/10.1080/00319100500303304

*Physics and Chemistry of Liquids*
Vol. 44, No. 1, February 2006, 45–59

Taylor & Francis
Taylor & Francis Group

# Association and molecular chain length effects on interfacial behavior§

A. MEJÍA*†, H. SEGURA†, J. WISNIAK‡
and I. POLISHUK‡

†Departamento de Ingeniería Química, Universidad de Concepción,
P.O. BOX 160-C-Correo 3, Concepción, Chile
‡Department of Chemical Engineering, Ben-Gurion University of the Negev,
Beer-Sheva 84105, Israel



(*Received in final form 2 May 2005*)

The scope of this work is to analyze the influence of the molecular chain length and association effects on the properties of vapor–liquid interfaces. Calculations are based on the gradient theory applied to the Statistical Associated Fluid Theory (SAFT) equation of state (EOS), yielding thus an approach that predicts both phase equilibrium and interfacial properties. In addition, the theoretical structure of the SAFT-EOS includes the specific effects under consideration. The approach proposed here is coherent with the density functional theory, although it is more direct to apply, and predictions are in good agreement with experimental data. Results show that the interface thickness decreases, while the interfacial tension increases, as the molecular chain length and/or the association degree increases at isothermal conditions. Such a trend may be explained in terms of the distortion of the cohesion energy. Detailed examples are discussed for subcritical binary mixtures and predictions are confronted with experimental data.

*Keywords*: Interfacial tension; Gradient theory; SAFT equation of state; Vapor–liquid equilibrium

## 1. Introduction

Fluid interfaces play a central role in many commercial and biological applications. Typical examples are processes that depend on adhesives, foams, colloids, coating, micelles and lipid bilayers. The design and control of these applications is based on the ability to modify interfacial properties, which are lumped on the magnitude of the interfacial tension ($\sigma$). Consequently, a theoretical approach able to describe the interfacial tension in terms of temperature ($T$), pressure ($P$), concentration ($x$) and chemical nature is valuable from a practical viewpoint. As follows from

*Corresponding author. Email: amejia@diq.udec.cl
§Partial results of this paper were presented at the 17th iupac conference on chemical thermodynamics, Rostock, Germany on July 28 – August 2, 2002.

*Physics and Chemistry of Liquids*
ISSN 0031-9104 print: ISSN 1029-0451 online © 2006 Taylor & Francis
DOI: 10.1080/00319100500303304

Rowlinson and Widom [1], the most successful approaches to describe the interfacial behavior are the gradient theory (GT) and the density functional theory (DFT). Briefly, these theories describe a continuous evolution of the density and Helmholtz energy along the interface, which are the basic information to predict $\sigma$ for fluid systems. The main difference between GT and DFT is the method that allows to calculate the interface concentration profile of each component ($\rho_i$) along the interface length ($z$) [1]. In particular, the GT predicts $\rho_i(z)$ by solving a set of partial differential equations that represent the condition of minimum energy at the interface. In contrast, typical DFT applications implicitly assume that $\rho_i$ is related to $z$ by a hyperbolic tangent function appropriately parametrized from the condition of minimum energy at the interface.

Results for pure fluids show that both GT and DFT approaches yield a suitable and similar picture of the structure of fluid interfaces and their properties [2–5]. However, the extension of these theories to predict interfacial properties of mixtures continues to be a challenging task. Previous works [2,3,6] demonstrate that the combination of the GT and equation of state (EOS) models is promising for correlating and/or predicting $\sigma$ in simple mixtures in a wide range of temperature conditions. A major part of the work on GT for mixtures has been devoted to the capability of the method to predict experimental information, although little attention has been given to the influence of the molecular structure on the interfacial behavior. In addition, no clear cut procedure exists concerning the application of DFT to mixtures, and the reason seems to be the way in which the approach generates the interfacial concentration profiles. For example, Telo da Gamma and Evans [7] claimed that the assumption of the shape of the concentration profile (in the case, of a hyperbolic tangent function), excludes the possibility of non-monotonic concentration profiles and conforms an artificial constraint which can be important to some mixtures. Anyway, it should be pointed out that the DFT has been effective in interpreting the effect of the molecular structure on the interfacial behavior of pure fluids, as demonstrated by Blas *et al.* [5].

The purpose of this work is to explore how the molecular structure affects the interfacial properties of fluid mixtures. Calculations are based on the GT applied to the SAFT-EOS, a model whose theoretical functionality includes the effect of the molecular chain length and association forces on macroscopic properties. Results are illustrated by analyzing the structure of the interface on the $z-\rho_i$ projection. The prediction capability is assessed by comparing the dependence of $\sigma$ on equilibrium variables ($P$ and $x$) with experimental data.



## 2. Theory

### 2.1. *The gradient theory for fluid interfaces*

The interfacial fluid between bulk phases in equilibrium obeys the constraint of minimum energy. According to the formalism of the GT, and for the case of a planar vapor–liquid interface, the former constraint can be expressed in terms of the following set of partial differential equations (PDEs) [2]

$$\sum_{j=1}^{n_c} \frac{\mathrm{d}}{\mathrm{d}z}\left(c_{ij}\frac{\mathrm{d}\rho_j}{\mathrm{d}z}\right) - \frac{1}{2}\sum_{i,l=1}^{n_c}\frac{\partial c_{lj}}{\partial \rho_i}\frac{\mathrm{d}\rho_l}{\mathrm{d}z}\frac{\mathrm{d}\rho_j}{\mathrm{d}z} = \frac{\partial \Phi}{\partial \rho_i} \quad i,j,l = 1,2,\ldots,n_c \tag{1}$$

where

$$\rho_i|_{z=-\infty} = \rho_i^v \quad \text{and} \quad \rho_i|_{z=\infty} = \rho_i^l$$

The solution of equation (1) is the concentration profile for each component $\rho_i(z)$ along the interface that allows to calculate the interfacial tension $\sigma$ according to the definition

$$\sigma = \int_{-\infty}^{\infty} \sum_{i,j=1}^{n_c} c_{ij} \frac{\mathrm{d}\rho_i}{\mathrm{d}z} \frac{\mathrm{d}\rho_j}{\mathrm{d}z} \mathrm{d}z \tag{2}$$

In equations (1) and (2), $n_c$ stands for the number of components, $z$ is a coordinate normal to the interface, $c_{ij}$ is the cross influence parameter, and $\rho_i$ is the concentration of component $i$ that, in turn, is related to the density of the mixture $\rho$ and the mole fraction $x_i$ by

$$\rho_i = x_i \rho \tag{3}$$

$\Phi$ corresponds to the *grand thermodynamic potential* defined as,

$$\Phi[\rho_i(z), \rho(z)] = a_0[\rho_i(z), \rho(z)] - \sum_{i=1}^{n_c} \rho_i(z) \mu_i^0 \left[T^0, V^0, \rho_i^0\right] \tag{4}$$

where $a_0$ is the density of the Helmholtz energy of the homogeneous system,

$$a_0 = \frac{A}{V} = RT\rho \left[ \int_0^{\rho} \left( \frac{P}{RT\rho^2} - \frac{1}{\rho} \right) \mathrm{d}\rho + \frac{1}{\rho} \sum_{i=1}^{n_c} \rho_i \ln \rho_i \right] \tag{5}$$

$\mu_i$ is the chemical potential of component $i$ and $T$ is the temperature. The superscript 0 denotes equilibrium condition at the bulk phase (liquid or vapor). $\mu_i$ can be determined from specific EOS models using equation (5) and the following relation

$$\mu_i = \left( \frac{\partial a_0}{\partial \rho_i} \right)_{T, V, \rho_{j \neq i}} \tag{6}$$

To this point, inspection of equations (1) to (6) reveals that the calculation of $\rho_i(z)$ between bulk phases depend on the EOS model and on the $c_{ij}$ values. The role of a specific EOS is to provide analytical relations for the Helmholtz energy and to predict the equilibrium state at which phases coexist.

In this work, $c_{ij}$ $(=c_{ji})$ is calculated using the procedure suggested by Carey [2]. Briefly, for the case of pure fluids, $c_{ii}$ $(i=j)$ is determined from experimental data of $\sigma$ as follows:

$$c_{ii} = \sigma_{\mathrm{exp}}^2 \left( \int_{\rho_v^0}^{\rho_l^0} \sqrt{2(\Phi + P^0)} \mathrm{d}\rho_i \right)^{-2} \tag{7}$$

The cross parameter $c_{ij}$ is calculated by averaging the pure component influence parameters according to

$$c_{ij} = (1 - \chi_{ij})\sqrt{c_{ii}c_{jj}} \qquad \chi_{ij} = \chi_{ji} = \begin{cases} 0 & \text{if } i = j \\ \chi_{ji} & \text{if } i \neq j \end{cases} \tag{8}$$

where $\chi_{ij}$ is an adjustable parameter, bounded to the range $0 \leq \chi_{ij} < 1$ [2,3,8]. In general, $c_{ii}$ depends on temperature and $\chi_{ij}$ can be estimated by smoothing experimental data of $\sigma$ for mixtures. When $\chi_{ij} = 0$, equations (1) simplify to the following set of algebraic equations (AEs)

$$\sqrt{c_{ii}}\left[\mu_k(\rho) - \mu_k^0\right] = \sqrt{c_{kk}}\left[\mu_i(\rho) - \mu_i^0\right] \qquad k = 1, 2, \ldots, i-1,\ i+1, \ldots, n_c \tag{9}$$

### 2.2. *The SAFT Model*

As follows from the version proposed by Huang and Radosz [9,10], the SAFT model is based on five additive contributions to the Helmoltz energy:

$$A(\rho, T) = A^{\text{ig}} + A^{\text{chain}} + A^{\text{hs}} + A^{\text{disp}} + A^{\text{ass}} \tag{10}$$

where $A^{\text{ig}}$ is the ideal gas reference, $A^{\text{chain}}$ accounts for the formation of molecule chains, $A^{\text{hs}}$ and $A^{\text{disp}}$ represent repulsion and dispersion interactions between the molecules, respectively, and $A^{\text{ass}}$ accounts for association forces. Pure components are characterized by five parameters: the molecular chain length (or number of segments) $m_i$, the segment volume $v_i^{\text{oo}}$, the temperature-dependent well-depth energy $u_i^{\text{o}}$ and the association energy $\varepsilon_i^{\text{AB}}$ and volumes $\kappa_i^{\text{AB}}$ between associating sites. The SAFT-EOS is extended to mixtures by applying quadratic mixing rules with an interaction parameter ($k_{ij}$) to the dispersion term. In addition, the association term for mixtures depends explicitly on association modes, which are well characterized for typical molecules in terms of the functional groups of the components.

### 2.3. *Typical patterns of the behavior at the interfacial region*

In previous sections we have discussed how the GT combined with an EOS model describes the behavior of the interfacial region and the interfacial tension in terms of the equilibrium state. The results of such an approach may be conveniently represented in the following two types of projections.

**2.3.1. $z - \rho_i$ projection.** The $z - \rho_i$ projection depicts the behavior of the concentration profiles of the species along the interface length, thus giving a picture of the structure of the interface. The availability of concentration profiles allows a direct comparison of the GT with alternative approaches, as the case of DFT and molecular dynamics results. From this projection it is possible to calculate the interface thickness and to observe adsorption (or desorption) of the species at the interface.

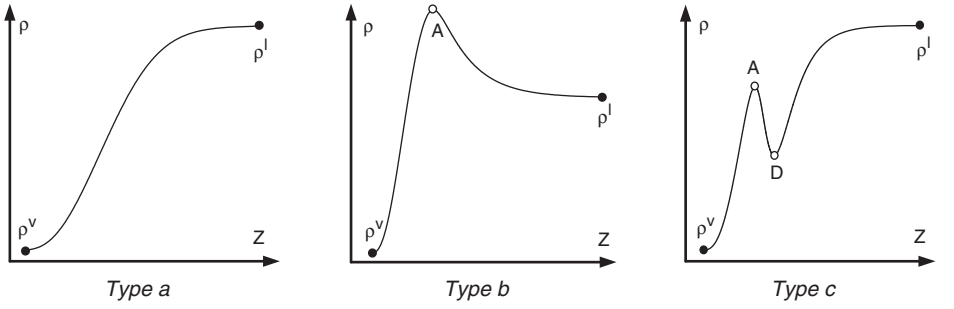


Figure 1. Schematic representation of concentration profiles for mixtures ($z-\rho_i$), (•) VLE bulk densities, (○) stationary points: A (adsorption) and D (desorption) of the species on the interfacial zone.

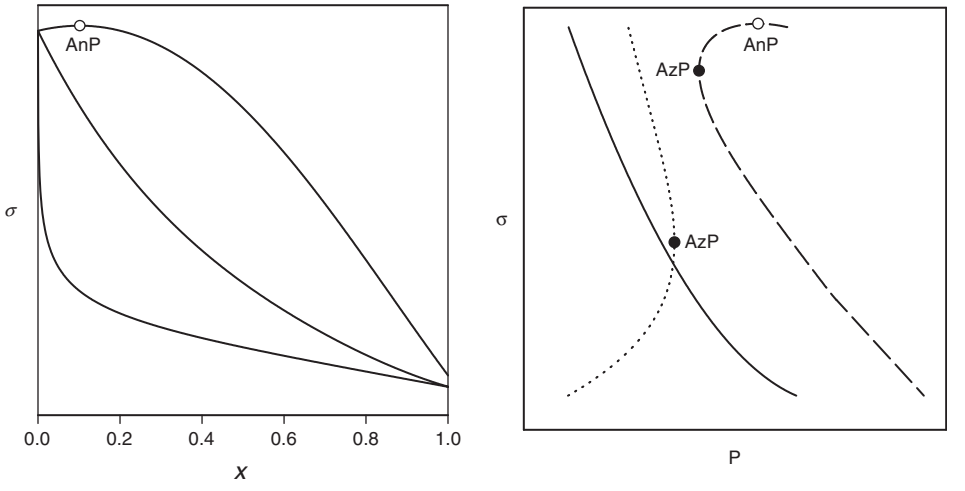


Figure 2. Schematic $P-\sigma$ and $x_1-\sigma$ plots for isothermal binary mixtures. (○) Aneotropic Point (*AnP*), (•) Azeotropic Point (*AzP*), (•••) mixtures with maxima vapor pressure azeotropes, (—) zeotropic mixtures, (–•–) mixtures with minima vapor pressure azeotropes.

Characteristic shapes of the $z-\rho_i$ projection are shown in figure 1, from which it is seen that along the interface width the concentration profile may be monotonic (*type a*) or non-monotonic (*type b* and *c*). In general, *type a* profiles are found in pure fluids and in mixtures of light n-alkanes. *Type b* profiles, in turn, are typical in mixtures of water + n-alkanes and mixtures of heavy n-alkanes. *Type c* profiles are characteristic of mixtures of alkanols + n-alkanes or amines. It should be pointed out that the non monotonic behavior of the concentration profiles *type b* and *c* is interesting because it reflects the surface activity at the interface. Non-monotonic profiles are characterized by stationary points which correspond to the interfacial point where adsorption (point A) or desorption (point D) of the species take place.

**2.3.2. $x-\sigma$, $P-\sigma$ projections.** The $x-\sigma$, and $P-\sigma$ projections, whose typical trends are shown in figure 2, relate the interface tension of a mixture with the conditions at which it exhibits phase equilibrium. These plots are useful to establish the accuracy

of $\sigma$ predictions and to analyze the relation of specific vapor–liquid equilibrium (VLE) features with the interfacial behavior. For the latter application it is useful to note that the slope of both projections is related by

$$\left(\frac{\partial\sigma}{\partial P}\right)_T = \left(\frac{\partial\sigma}{\partial x}\right)_T \left(\frac{\partial P}{\partial x}\right)_T^{-1} \tag{11}$$

Depending on the chemical nature of the components of a mixture, the projections in question may show two types of significant stationary points: aneotropes and azeotropes. Aneotropic points (*AnP*) are characterized by the condition that $[\partial\sigma/\partial x]_T = 0$. Hence, and as follows from equation (11), the existence of aneotropes implies stationary points both in the $x-\sigma$ and $P-\sigma$ projections. In a similar manner, for the case of azeotropes where $[\partial P/\partial x]_T = 0$, equation (11) predicts that $[\partial P/\partial\sigma]_T = \infty$ in the $P-\sigma$ projection.



## 3. Procedure for calculations

The calculation of $\sigma$ proceeds by calculating the interfacial properties of pure components and, then, by extending the approach to mixtures. A basic requirement for both steps is the capability of the EOS model to accurately predict VLE of the mixture and its components. In the version presented by Huang and Radosz [9,10], the parameters of the SAFT-EOS are sufficient for calculating the VLE of pure components. For the case of mixtures, interaction parameters are usually required to correlate experimental VLE data. Once the model has been tuned to experimental VLE data, the following procedure may be used for calculating interfacial properties:

*Step 1* Calculation of influence parameters for pure fluids $c_{ii}$

- Given $T^0$ and the EOS parameters for pure fluids, calculate the $P^0$ and the saturation densities $\rho^{0,\mathrm{L}}$, $\rho^{0,\mathrm{V}}$. The pure component vapor pressure algorithm proposed by Segura and Wisniak [11] has been found effective for the purpose.
- From the experimental value of the interfacial tension $\sigma_{\mathrm{exp}}$, calculate $c_{ii}$ at $T^0$ using equation (7).
- The same procedure may be repeated for the whole temperature range in which $\sigma_{\mathrm{exp}}$ data are available. For a pure fluid, $c_{ii}$ depends on temperature. So, as pointed out by Carey [2], it is convenient to consider that the temperature dependence of $c_{ii}$ is usually well smoothed by a linear relation.

*Step 2* Calculation of interfacial properties for mixtures

- Specify $T^0$ and the liquid phase mole fraction $x_i$. Then, perform a bubble point calculation to predict $P^0$, the vapor phase mole fractions $y_i$ and the bulk densities $\rho^{0,\mathrm{L}}$, $\rho^{0,\mathrm{V}}$. In this case, the SAFT-EOS is used for predicting the equilibrium state and the $\phi-\phi$ approach is considered for performing VLE calculations [12].
- Calculate $c_{ij}$ from equation (8) assuming initially that $\chi_{ij} = 0$.
- Solve the AEs in equation (9) (if $\chi_{ij} = 0$) or the PDEs in equation (1) (if $\chi_{ij} \neq 0$) to obtain the concentration profile $\rho_i(z)$.

- Calculate the interfacial tension $\sigma$ of the mixture according to its integral definition in equation (2).
- Test other $\chi_{ij}$ values ($0 \leq \chi_{ij} < 1$) values to minimize deviations if the prediction of $\sigma$ is not satisfactory.

## 4. Results and discussions

Following the objective of this work, we have considered mixtures of hexane + n-alkanes with increasing carbon number to analyze the influence of the molecular chain length on interfacial properties. Association effects have been taken into account by considering mixtures of cyclohexane + associating or non-associating components. Although this selection of components and mixtures is arbitrary, it satisfies some requirements concerning the availability of experimental data for $\sigma$. In addition, the SAFT model is reliable for predicting the VLE of the selected components. Table 1 summarizes physical properties and parameters of the SAFT model for pure components while table 2 presents parameters for binary mixtures and deviation statistics for VLE predictions. From table 2 it is seen that, for group of mixtures considered in this work, the SAFT-EOS predicts accurate VLE with average percentage deviations lower than 2% in pressure and 0.92% in vapor phase mole fraction.



Table 1. Physical properties of the pure components.[a]

| Fluid | $m_i$ | $v_i^{oo}$ (mL mol$^{-2}$) | $u_i^o$ ($\kappa$ K$^{-1}$) | $\varepsilon_i^{AB}$ ($\kappa$ K$^{-1}$) | $10^2 \times \kappa_i^{AB}(\kappa)$ | $T$ (K) | $10^{20} \times c_{ii}$ (J m$^5$ mol$^{-2}$) |
|---|---|---|---|---|---|---|---|
| Benzene | 3.749 | 11.421 | 250.19 | 0 | 0 | 303.15 | 20.9997 |
| Butanoic acid | 3.800 | 13.000 | 268.93 | 4155 | 0.370 | 303.15 | 13.9190 |
| n-butanol | 3.971 | 12.000 | 225.96 | 2605 | 1.639 | 303.15 | 13.7620 |
| Cyclohexane | 3.970 | 13.502 | 236.41 | 0 | 0 | 303.15 | 34.7028 |
| Decane | 7.527 | 11.723 | 205.46 | 0 | 0 | 313.15 | 82.5242 |
| Heptane | 5.391 | 12.282 | 204.61 | 0 | 0 | 313.15 | 43.8602 |
| Hexane | 4.724 | 12.475 | 202.72 | 0 | 0 | 313.15 | 35.6556 |
| Octane | 6.045 | 12.234 | 206.03 | 0 | 0 | 313.15 | 57.1874 |
| Tetradecane | 9.978 | 12.389 | 209.40 | 0 | 0 | 313.15 | 172.1429 |

[a] Pure fluid parameters of the SAFT-EOS have been taken from Huang and Radosz [9]. The association types are 1 for butanoic acid, 2B for n-butanol and 0 for the other fluids. $c_{ii}$ are fitted at $T$ from experimental $\sigma$ data, which are taken from Wohlfarth and Wohlfarth [13].

Table 2. Binary parameters for mixing rules and statistic deviations in vapor pressure and vapor phase mole fractions for VLE correlations and interfacial tensions predictions.

| System | $T$ (K) | $k_{ij}$[a] | AADP%[b] | $\Delta y_1$[c] | AAD$\sigma$ %[b] |
|---|---|---|---|---|---|
| Hexane + Heptane | 313.15 | −0.0050 | 1.3 | 0.01 | 0.4 |
| Hexane + Octane | 313.15 | −0.0067 | 1.7 | 0.1 | 0.5 |
| Hexane + Decane | 313.15 | −0.0013 | 2.0 | 0.05 | 1.2 |
| Hexane + Tetradecane | 313.15 | 0 | 1.7 | 0.03 | 0.7 |
| Cyclohexane + Benzene | 303.15 | 0.0199 | 0.2 | 0.2 | 0.2 |
| Cyclohexane + Butanoic acid | 303.15 | 0.0300 | 1.8 | 0.03 | 0.2 |
| Cyclohexane + n-butanol | 303.15 | 0.0181 | 1.6 | 0.9 | 0.1 |

[a] The $k_{ij}$ parameters are fitted from experimental VLE data, which are taken from Maczynski *et al.* [14]. [b] Absolute Average Deviation in Pressure (AAD) is the absolute average deviation, $\text{AAD}\delta = (100/N_P)\ \Sigma_{i=1,N_p}\ |\delta_i^{exp} - \delta_i^{cal}|/\delta_i^{exp} (\delta = P,\ \text{or}\ \sigma)$. [c] $\Delta y_1 = (100/N_P)\ \Sigma_{i=1,N_p}\ |y_i^{exp} - y_i^{cal}|$. $N_P$ is the number of experimental points. VLE deviations are measured with respect to the experimental data used for $k_{ij}$ and the $\sigma$ deviations are measured respect to the experimental $\sigma$ data, which are taken from Wohlfarth and Wohlfarth [13].

As indicated previously, $c_{ii}$ values and a model capable to predict VLE provide all the information needed to describe the interfacial behavior. Using $\chi_{ij}=0$ for all the mixtures considered in this work, the maximum deviation of $\sigma$ was 1.2% (see table 2). For this reason, although a marginal and non-statistically significant improvement of $\sigma$ predictions may be obtained from optimal $\chi_{ij}$ values, *we set this mixture parameter to its zero value*. It should be pointed out that optimal $\chi_{ij}$ values are very close to zero and, additionally, concentration profiles show equivalent trends when comparing with the case in which $\chi_{ij}=0$.

Deviation statistics in table 2 confirm that both the VLE and $\sigma$ can be predicted from the GT combined with SAFT-EOS. Based on the good agreement of predictions with experimental data (see table 2), we claim that our approach yields a reliable description of the influence of the molecular chain length and association forces on interfacial properties.

### 4.1. *Influence of the molecular chain length on interfacial properties*

The influence of the molecular chain length is illustrated by considering isothermal mixtures ($T=313.15$ K) of hexane (1) + n-alkanes (2) with increasing carbon number. Figure 3 shows the characteristic $z-\rho_i$ projections for these mixtures. From the figure in question we can observe that:

- As $x_1$ increases, the slope of the $z-\rho_1$ curve increases and the surface activity of hexane decreases, as reflected on the stationary points of the profile.
- As the molecular chain length increases, the surface activity of hexane increases and the interface width decreases.
- At constant mole fraction, the slope of the $z-\rho_1$ curve increases and the slope of the $z-\rho_2$ curve decreases as the chain length increases.
- At constant mole fraction, as the molecular chain length increases the surface activity increases and the interface length decreases. This last effect can be appreciated better in figure 4, which depicts the interface length as a function of the carbon number of the second component.

Figures 5a, b compare $\sigma$ predictions with experimental data taken from Wohlfarth and Wohlfarth [13] for the mixtures under consideration. Inspection of these figures reveal that good predictions of $\sigma$ are obtained in the whole range of $P$ and $x_1$. It is also seen that the interfacial tension increases with the molecular chain length, a behavior that can be explained in terms of the reduction of the interface thickness.

All the previous trends may be explained in terms of the increment of the cohesion energy, as the C atoms increases.

### 4.2. *Influence of association on interfacial properties*

The effect of the association is illustrated by considering isothermal mixtures of cyclohexane with associating solvents of similar chain lengths at 303.15 K. The second component self-associates according to modes type 0 (benzene), 1 (methanol) or 2B (butanoic acid) in the classification of Huang and Radosz [9]. As a reference, self-association mode type 1 exhibits larger association energy and lower association volume than the mode type 2B. No association behavior is observed for mode type 0.

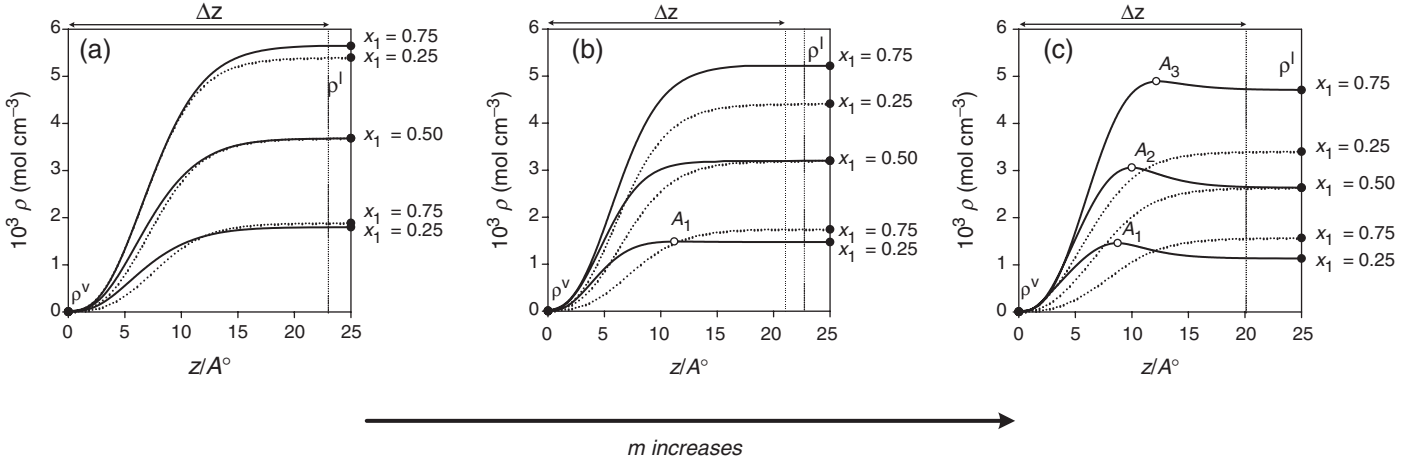


Figure 3. Concentration profiles ($z-\rho_i$) for hexane mixtures at 313.15 K. (—) $z-\rho_1$, (●●●) $z-\rho_2$, (●) VLE bulk densities, (○) stationary points: $A_1-A_3$ adsorption of species on the interfacial zone, $\Delta z$ interfacial zone, (a) hexane (1) + heptane (2), (b) hexane (1) + decane (2), (c) hexane (1) + tetradecane (2).

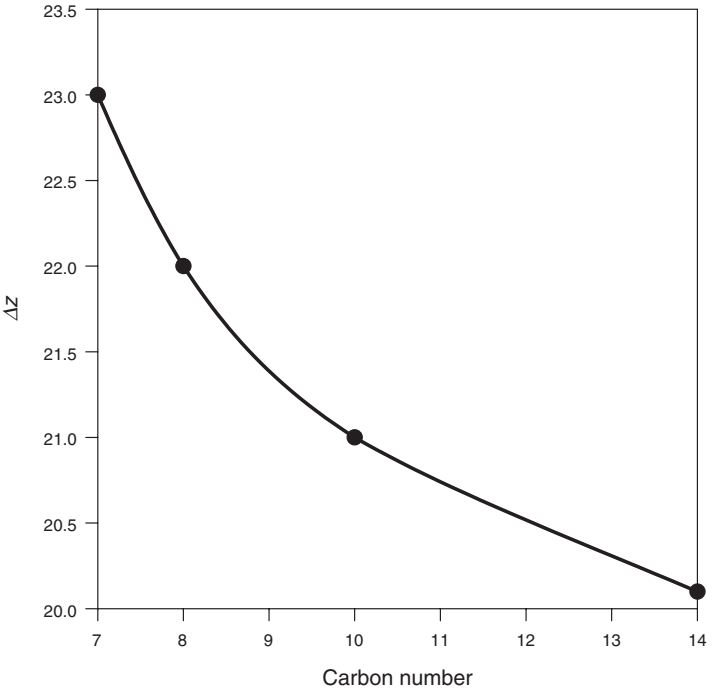


Figure 4. Variation of the interface width ($\Delta z$) as a function of carbon number.



At the $z-\rho_i$ projection, cyclohexane mixtures show a dependence of concentration profiles on $x_i$ similar to the case of non-associating mixtures presented in section 4.1. This means that as $x_1$ increases, the slope of the $z-\rho_1$ curve increases and the surface activity of cyclohexane decreases. However, associating mixtures show a different patterns than non-associating mixtures. In fact, this kind of mixtures exhibit both adsorption and desorption at the interface length, as described next. Figure 6 show the $z-\rho_i$ projection for cyclohexane mixtures at $x_1=0.50$. For each system we can observe the following patterns:

- Associated mixtures exhibit stronger surface activity than non-associating mixtures.
- The associating component (2) always exhibits adsorption (points $A_1$ and $A_2$) and the non-associating fluid (1) shows both adsorption and desorption (point D) at the interface.
- As the association energy, $\varepsilon_i^{AB}$, decreases, the surface activity and the interface length increase.
- As the association volume, $\kappa_i^{AB}$, increases, the surface activity and the interface length decrease.

From the previous result, we can observe that the structure of the interface and the interfacial tension is significantly influenced by the distortion of the cohesion energy induced by association forces' influences.

Figures 7a and b compare $\sigma$ predictions with experimental data [13] for cyclohexane mixtures. From these figures we can conclude that a good prediction of $\sigma$ is obtained for each mixture in all the $P$, $x_1$ range. In addition, inspection of these figures revel

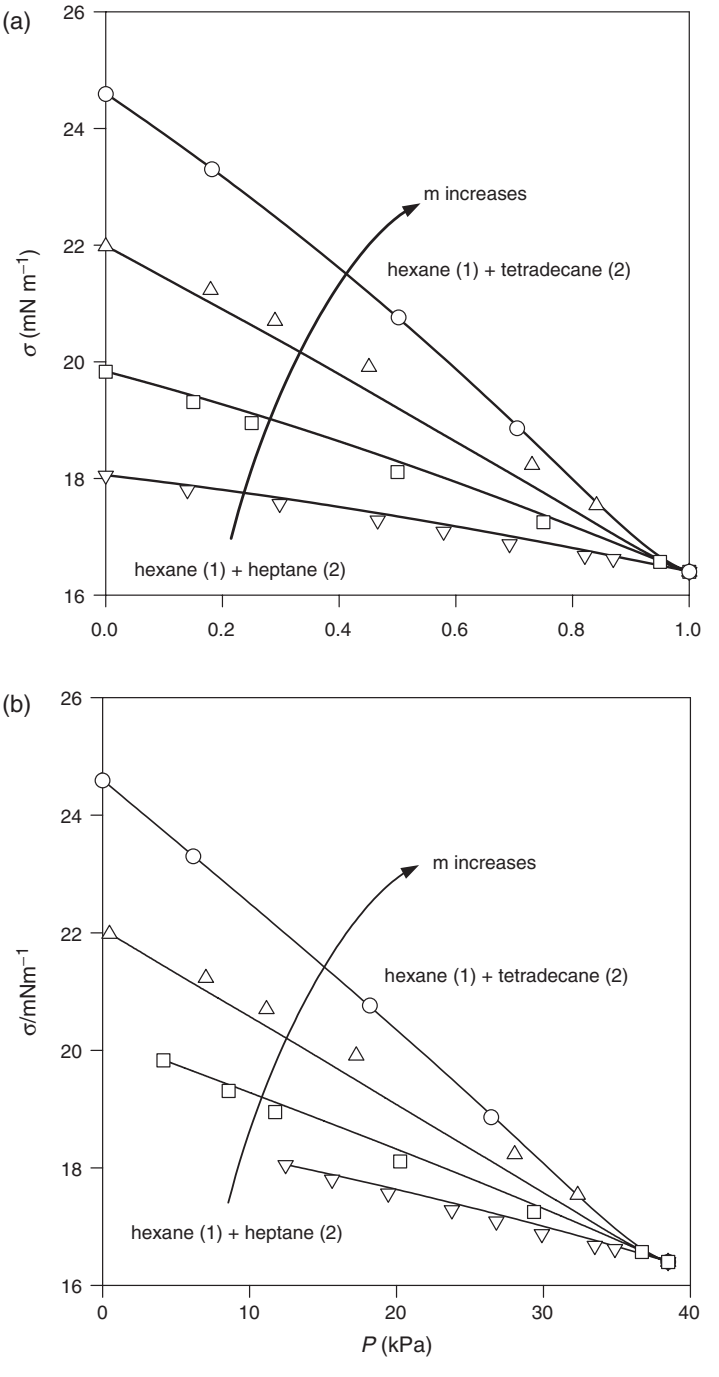


Figure 5. (a) $x_1 - \sigma$ projections for hexane mixtures at 313.15 K. (b) $P - \sigma$ projections for hexane mixtures at 313.15 K. (—) GT + SAFT, (▽, □, △, ○) Experimental $\sigma$ data [13]: (▽) hexane (1) + heptane (2), (□) hexane (1) + octane (2), (△) hexane (1) + decane (2), (○) hexane (1) + tetradecane (2).

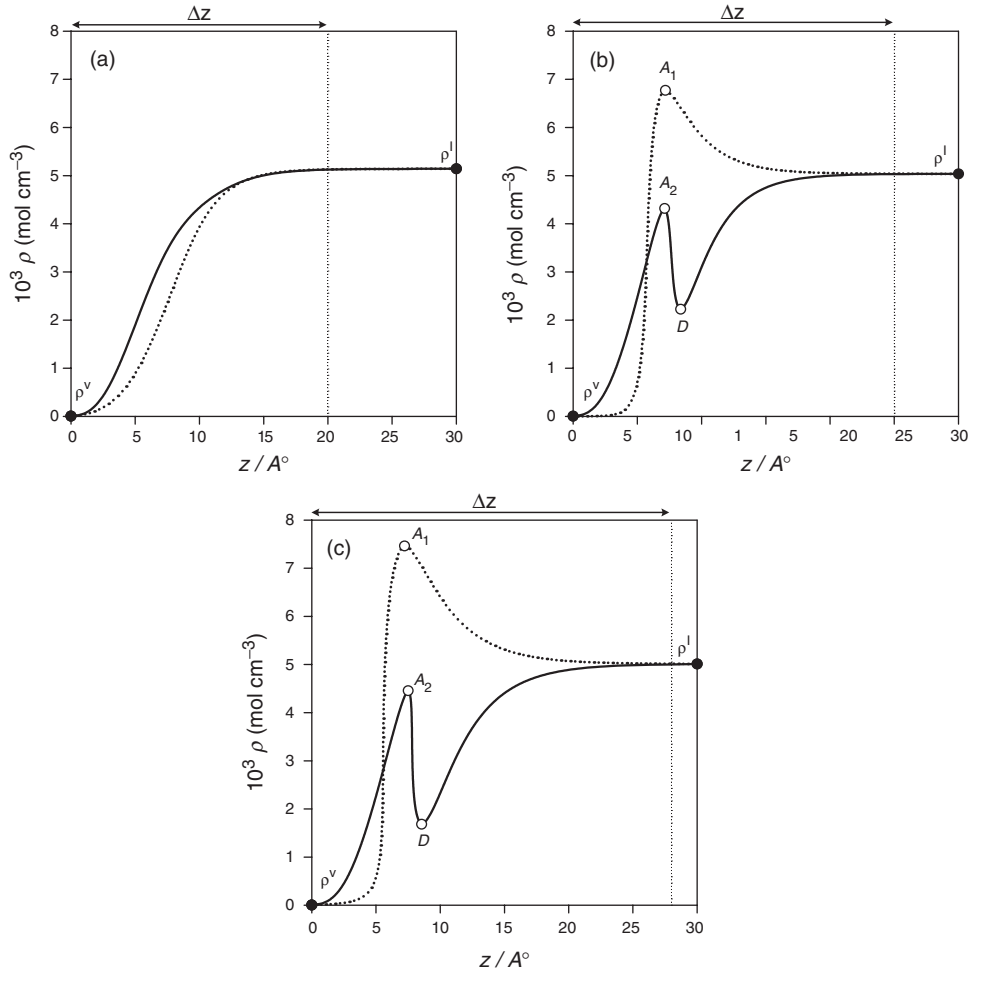


Figure 6. Concentration profiles ($z-\rho_i$) for cyclohexane mixtures at 303.15 K and $x_1=0.5$. (—) $z-\rho_1$, (●●●) $z-\rho_2$, (●) VLE bulk densities, (◯) stationary point: $A_1$, $A_2$ adsorption and D desorption of species on the interfacial zone. (a) cyclohexane (1) + benzene (2), (b) cyclohexane (1) + butanoic acid (2), (c) cyclohexane (1) + n-butanol (2).

that as the association energy decreases and the association volume increases, the interfacial tension of the mixture decreases. In fact, mixtures with self-associating components exhibit lower interface tensions when association forces decrease.

## 5. Concluding remarks

In this work we have analyzed the influence of the molecular chain length and of association forces on the properties of vapor–liquid interfaces for binary mixtures. The SAFT-EOS has been used for predicting equilibrium properties and interfacial tensions have been calculated from the GT. According to the results obtained,

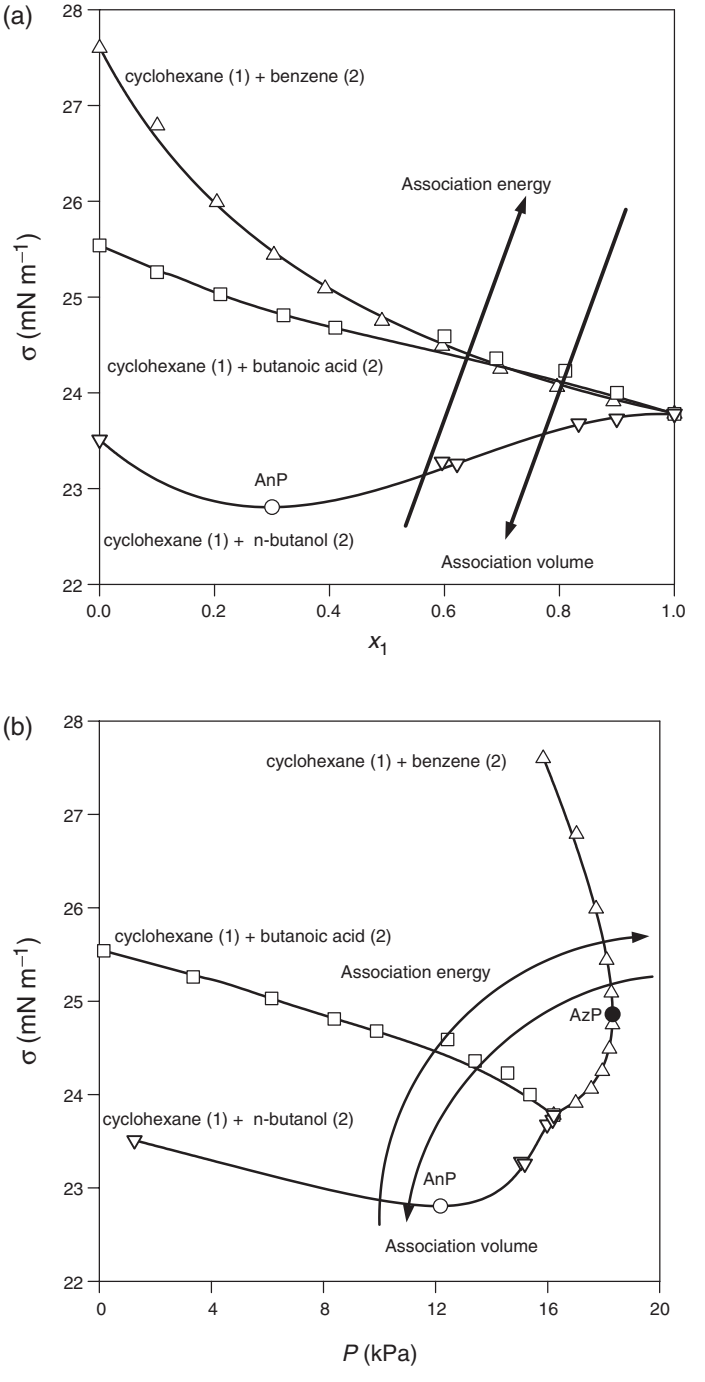


Figure 7. (a) $x_1 - \sigma$ projections for cyclohexane mixtures at 303.15 K. (b) $P - \sigma$ projections for cyclohexane mixtures at 303.15 K. (—) GT + SAFT, (▽, □, △, ○) Experimental $\sigma$ data [13]: (△) cyclohexane (1) + benzene benzene (2), (□) cyclohexane (1) + butanoic acid (2), (▽) cyclohexane(1) + n-butanol (2), (○) Aneotropic (AnP) and (●) Azeotropic Points (AzP).

a suitable prediction of $\sigma$ is obtained both for associating and non-associating mixtures. The magnitude of the cohesion energy (that depends on molecular chain length and/or association modes) influences significantly the interface structure. The effects of the cohesion energy on the interfacial behavior of the mixtures analyzed in this work are similar to that discussed by Blas *et al.* [5] for pure fluids. Specifically we have found the following effects:

*Non-associating mixtures*: As the molecular chain length increases, the surface activity increases and the interface width decreases, implying thus that the interface tension of the mixture increases.
*Associating mixtures*: These mixtures are characterized by a stronger surface activity than non-associating mixtures. At the interface region, the self-associating component exhibits adsorption, while the non-associating component exhibits both adsorption and desorption. Finally, when the association energy (well depth) and/or the association volume (well width) decrease, the surface activity and the interface length increase and, consequently, the interface tension decreases. Unfortunately, due to the lack of systematic experimental information of VLE and $\sigma$ that allow to analyze independently both association effects in the interfacial behavior, we are unable to conclude that previous patterns are the general behavior to associates mixtures.



## List of symbols

| | |
|---|---|
| $A^{\text{ass}}$ | association Helmholtz energy |
| $A^{\text{chain}}$ | molecular Helmholtz energy |
| $A^{\text{disp}}$ | dispersive Helmholtz energy |
| $A^{\text{hs}}$ | repulsive Helmholtz energy |
| $A^{\text{ig}}$ | ideal gas Helmholtz energy |
| $a_0$ | Helmholtz energy density of the homogeneous system |
| $c$ | influence parameter |
| $\kappa$ | Boltzmman constant |
| $k_{ij}$ | interaction parameter for a mixing rule |
| $m$ | molecular chain length |
| $n_c$ | number of components |
| $P$ | absolute pressure |
| $R$ | universal gas constant |
| $T$ | absolute temperature |
| $u_i^{\text{o}}$ | the temperature sensitive well depth |
| $V$ | volume |
| $v_i^{\text{oo}}$ | segment volume |
| $x$, $y$ | mole fraction of the liquid and vapor phases |
| $z$ | distance normal to the interface |

## Greek

| | |
|---|---|
| $\chi$ | adjustable parameter |
| $\varepsilon_i^{\text{AB}}$ | association energy between two associating sites AB |
| $\Phi$ | grand thermodynamic potential |

$\kappa_i^{AB}$ association volume between two associating sites AB
$\mu$ chemical potential
$\rho$ molar concentration
$\sigma$ interfacial tension

## Subscripts

exp experimental data
$i, j, l, k$ species
$m$ mixture
$s$ independent variable

## Superscripts

L liquid
V vapor
0 equilibrium



## Acknowledgments

This work was financed by FONDECYT, Santiago, Chile (Project 1050157). Partial founding by the Israeli Science Foundation, Grant Number 340/00, are also acknowledged. A.M. acknowledges to MECESUP project (UCO 0108) for financing the Landolt–Börnstein data bases.

## References

[1] J.S. Rowlinson, B. Widom. *Molecular Theory of Capillarity*, Oxford University Press, Oxford (1989).
[2] B.S. Carey. The gradient theory of fluid interfaces. Ph.D. Thesis, University of Minnesota (1979).
[3] P.M.W. Cornelisse. The gradient theory applied, simultaneous modelling of interfacial tension and phase behaviour. Ph.D. Thesis, Delft University (1997).
[4] H. Kahl, S. Enders. *Fluid Phase Equilibria*., **172**, 27 (2000).
[5] F.J. Blas, E. Martín del Río, E. de Miguel, G. Jackson. *Molec. Phys*., **99**, 1851 (2001).
[6] H. Kahl, S. Enders. *Phys. Chem. Chem. Phys*., **4**, 931 (2002).
[7] M.M. Telo da Gamma, R. Evans. *Molec. Phys*., **48**, 229 (1983).
[8] H.T. Davis, L.E. Scriven. *Adv. Chem. Phys*., **49**, 357 (1982).
[9] S.H. Huang, M. Radosz. *Ind. Eng. Chem. Res*., **29**, 2284 (1990).
[10] S.H. Huang, M. Radosz. *Ind. Eng. Chem. Res*, **30**, 1994 (1990).
[11] H. Segura, J. Wisniak. *Computers Chem. Eng*., **21**, 1339 (1997).
[12] H. Orbey, S.I. Sandler. *Modeling Vapor Liquid Equilibria: Cubic Equations of State and their Mixing Rules*, Cambridge University Press, New York (1998).
[13] Ch. Wohlfarth, B. Wohlfarth. Numerical data and functional relationships in science and technology. *Surface Tension of Pure Liquids and Binary Liquid Mixtures*, in Landolt–Börnstein, New Series Group IV Physical Chemistry, M.D. Lechner (Ed.), Vol. 16, pp. 23–34, Springer Verlag, Berlin, Heidelberg (1997).
[14] A. Maczynski, Z. Maczynska, A. Skrzecz. *Floppy Book on Vapor–Liquid Equilibrium Data in Binary Systems*, V. 1991.07.30, Polish Academy of Sciences. Institute of Physical Chemistry, Warszawg and Institute of Carbochemistry, Gliwice.